Journal of Applied Electrochemistry **30**: 499–506, 2000.

Hydrogen evolving activity on nickel–molybdenum deposits using experimental strategies

C.-C. HU* and C.-Y. WENG
Department of Chemical Engineering, National Chung Cheng University, Chia-Yi, 621 Taiwan
*(*author for correspondence)*

Received 11 May 1999; accepted in revised form 24 November 1999

Key words: citrate electrolyte, fractional factorial design, hydrogen evolution, Ni/Mo-deposits

Abstract

Hydrogen evolution on various Ni–Mo deposits was systematically compared using fractional factorial design (FFD) and response surface methodology (RSM). The electroplating variables such as pH, Ni/Mo atomic ratio and citrate concentration were found to be the key factors affecting the hydrogen evolution activity from the FFD study. The effects of Ni/Mo atomic ratio and citrate concentration in the plating bath on the apparent current density, the exchange current density, and the specific activity (based on i/q^*) of hydrogen gas evolution, and on the Mo/(Ni + Mo) ratio of the deposits were examined using regression models. These models, represented as response surface contour plots, showed the maximum hydrogen evolving activity occurring on the Ni–Mo deposit electroplated from the bath with a pH of 8, a Ni/Mo ratio of 3.3 and a citrate concentration of 40 g l^{-1}, respectively.

1. Introduction

Hydrogen is a potential future candidate as an efficient and inexpensive energy carrier due to its recyclable and nonpolluting nature and the fact that it is available in practically unlimited quantity (e.g., [1]). The high activation overpotential of the hydrogen evolution reaction (HER) and the poisoning problem for the underpotential deposition (UPD) of trace metal ions [2, 3], has attracted much interest in the development of better electrocatalysts and longer service-life cathodes (e.g., [4]).

Promising electrode materials for most commercial electrolysers in alkaline media can be grouped as noble metal black, Raney-type nickel, nickel alloy and nickel compounds [2, 5–7]. Based on the criteria of activity and stability at an acceptable cost, the latter three kinds of electrode are preferable. Hydrogen evolution has been found to depend strongly on the characteristics of the electrocatalytic surface [8, 9] and the incorporation of adsorbed hydrogen atoms [9, 10]. Nickel–molybdenum deposits are particularly important for this reaction because they have been found to be the best electrocatalyst among several nickel alloys [11]. Moreover, according to the Engel–Brewer valence-bond theory [5, 12, 13], whenever transition metals with empty or less-filled d orbitals (e.g., Mo) are alloyed with those with more-filled d orbitals (e.g., Ni), a synergistic effect in the hydrogen-evolving activity of these materials is expected. Accordingly, there should exist an optimal activity for hydrogen evolution on Ni–Mo deposits when nickel and molybdenum are codeposited.

Since pure molybdenum can not be directly electroplated from aqueous solutions [14], nickel–molybdenum alloy plating has been recognized as an induced codeposition. In addition, the induced codeposition of molybdenum with nickel has been shown that the composition of molybdenum within the deposits may be controlled by the relative concentrations, mass transport of either molybdate or nickel species [15], the concentration of citrate [16], pH [17], and bath temperature [14]. Several hypotheses therefore have been suggested to explain the complicated induced codeposition mechanism [14, 15, 17–19].

The purpose of this work is to identify optimum electroplating conditions to produce Ni–Mo deposited electrodes with the highest hydrogen-evolving activity in the alkaline media. To evaluate efficiently the key electroplating variables affecting the hydrogen-evolving activity of Ni–Mo deposits, fractional factorial design (FFD) was first employed [20]. The response surface methodology (RSM) coupled with central composite design (CCD) [20, 21] was used to determine the optimum conditions in electroplating Ni–Mo deposits exhibiting the highest apparent current density (i.e., activity) for hydrogen evolution. The specific activity (based on unit area) of hydrogen evolution and the molybdenum content within the deposits were subsequently determined and subjected to regression since the hydrogen-evolving activity may be linked to the composition and/or structure of Ni–Mo alloys, which

should depend on the electroplating variables. Ideally, this work provides a further understanding of the influences of molybdenum content within the Ni–Mo alloys on the apparent and specific activities for hydrogen evolution.

2. Experimental details

Nickel–molybdenum deposits were electroplated onto commercial pure (99.5%) 1 cm × 2 cm copper plates. These copper plates were first cleaned with trichloroethylene, rinsed with pure water, and then, anodized at 40 mA cm^{-2} in a 0.1 M NaOH solution for 10 min. After anodizing, the plates were cathodically polarized at 40 mA cm^{-2} in another 0.1 M NaOH solution for 1 min, vibrated in an ultrasonic bath for 5 min, acid-cleaned with 0.1 M HCl for 2 min, and finally rinsed with pure water. After cleaning, the Cu substrate was vertically placed at the center of an electroplating cell between two parallel nickel plates with a total geometric area of 32 cm^2. The total concentration of Ni and Mo ions in the plating bath was kept constant (0.5 M). The plating baths mainly consisted of $NiSO_4.6H_2O$ (Wako E.P.), $Na_2MoO_4.2H_2O$ (Hanawa E.P.), and $Na_2C_6H_5O_7.2H_2O$ (Hanawa E.P.) with pH adjusted by NH_4OH. The plating baths were stirred by a 5 cm magnetic bar on a magnetic stirrer at a constant rate during electroplating. The effects of the following electroplating variables were investigated in the FFD study: (A) temperature; (B) current density; (C) pH; (D) Ni/Mo ratio; and (E) sodium citrate concentration on the hydrogen evolving activity of various Ni–Mo deposits. Fixed levels of these five variables are listed in Table 1, with design levels being given in Table 2. Note that in the CCD study, two additives (saccharin ($C_7H_5NO_3S$), 0.2 g l^{-1} and tetrabutyl-ammonium bromide, 0.1 g l^{-1}) were added to all plating solutions to reduce the internal stress of the deposits and to improve the adhesion for long-time water electrolysis. The electroplating was stopped when the passed charge was equal to 20 C cm^{-2}. The exposed geometric area of each cathode prepared for electrochemical studies was 1 cm^2 by means of double coatings of epoxy resin and polytetrafluorene ethylene (PTFE).

The average composition of various Ni–Mo deposits in the CCD design was measured by an energy-dispersive X-ray (EDX) spectroscope at three points using a scanning electron microscope (SEM, Jeol JSM35). In addition, X-ray diffraction analysis (XRD: Rigaku X-ray diffractometer using a Cu target) revealed that all Ni–Mo deposits in the CCD study have an amorphous structure (not shown here).

Table 1. Factors and levels for 2^{5-1} fractional factorial design

Factor		Level	
		−1	+1
A	Temperature/°C	20	50
B	Current density/A m^{-2}	500	2000
C	pH	8	11
D	Ni/Mo ratio	3/2	22/3
E	Citrate concentration/g l^{-1}	60	120

Table 2. Design matrix and experimental data for hydrogen evolving activity of 2^{5-1} fractional factorial design with the defining relation I = ABCDE

Run	Factor					i/mA cm^{-2} ($\eta \approx 230$ mV)
	A	B	C	D	E	
1	−1	−1	−1	−1	+1	32.58
2	+1	−1	−1	−1	−1	42.36
3	−1	+1	−1	−1	−1	65.01
4	+1	+1	−1	−1	+1	46.56
5	−1	−1	+1	−1	−1	16.56
6	+1	−1	+1	−1	+1	7.5
7	−1	+1	+1	−1	+1	14.76
8	+1	+1	+1	−1	−1	15.24
9	−1	−1	−1	+1	−1	49.89
10	+1	−1	−1	+1	+1	19.72
11	−1	+1	−1	+1	+1	8.45
12	+1	+1	−1	+1	−1	40.93
13	−1	−1	+1	+1	+1	11.46
14	+1	−1	+1	+1	−1	5.33
15	−1	+1	+1	+1	−1	12.65
16	+1	+1	+1	+1	+1	10.14

The activity (i.e., apparent current density, i) of hydrogen evolution on different Ni–Mo deposits was compared at the same overpotential ($\eta \approx 230$ mV) from the Tafel curves of the HER. All Tafel curves were measured by a pseudo steady-state polarization method through means of an electrochemical analyser system, BAS-100W (Bioanalytic System, Inc., USA) in a three-compartment cell. During this study, the electrode potentials were first set at −1020 mV ($\eta \approx 0$ mV) for 10 min and then scanned at 0.5 mV s^{-1} to −1300 mV ($\eta \approx 280$ mV). Note that the log i/E curve would follow the same trace after 4–5 applications of this cathodic polarization. In addition, all Tafel curves were measured with iR correction. In all electrochemical measurements, an Ag/AgCl electrode (Argenthal, 3 M KCl, 207 mV *vs* SHE at 25 °C) was used as the reference, while a platinum wire with an exposed surface area equal to 2 cm^2 was employed as the counter electrode. A Luggin capillary, whose tip was set at a distance of about 1–2 mm from the surface of working electrode, was used to minimize errors due to iR drop in the electrolytes.

All solutions were prepared with pure water produced by a reagent water system (Milli-Q SP, Japan) at 18 MΩ cm and all reagents not specified in this work were Merck, GR. In addition, the 1 M NaOH solution used to compare the hydrogen evolving activity and to obtain the voltammetric charges of all deposits in the working-electrode compartment was degassed with purified nitrogen gas for 25 min before the electrochemical measurements. This nitrogen gas flowed over the solution during these measurements. Solution temperature not specified was maintained at 25 °C with an accuracy

of 0.1 °C by means of a water thermostat (Haake DC3 and K20).

3. Results and discussion

3.1. *Fractional factorial design*

To efficiently find the key variables affecting the activity of hydrogen evolution on Ni–Mo deposits, fractional factorial design (FFD) was introduced to screen out these key variables. This experiment design can find the influences of each preparation variable at a variety of other variable levels, as well as the interactions among these variables on the hydrogen-evolving activity.

The design factors and levels for the 2^{5-1} FFD experiments are listed in Table 1 meanwhile the design matrix and results (column 7) are shown in Table 2. According to the defining relation I = ABCDE introduced by Box et al. [20], the estimate of main effect for factor E is identical to that of the four-factor interaction, ABCD, effect. Therefore, the main effect of factor E and the interaction effect of ABCD are said to be confounded [20, 22]. Since the high-order interactions (e.g., three-, four-, and five-order) do not exist in usual and the resolution of this design is V [22], the main effect of factor E can be isolated from the confounded effects by this FFD experiment. Similar situations were also held for factors A, B, C and D.

Calculation of main and interaction estimates of the electroplating variable effects followed the procedure recommended by Box et al. [20]. The results of main effect for factors A to E are shown in Figure 1. This figure shows that the effects of C (pH), D (Ni/Mo ratio) and E (citrate concentration), especially bath pH, are the key variables affecting the activity of Ni–Mo deposits for hydrogen evolution. For Ni–Mo induced deposition, a basic plating bath pH has been proposed to be an important variable influencing the quality and composition of the deposits because of the presence of free NH_3 [14, 17]. The Mo content of Ni–Mo deposits also increases with increasing Mo/Ni ratio in the bath [14, 15, 23]. The formation and structure of the Ni/Mo complex have been found to be affected by the citrate concentration [16], which probably causes a change in composition and/or structure of Ni–Mo deposits. Accordingly, the composition and/or structure of Ni–Mo deposits should depend on pH, Ni/Mo ratio and citrate concentration. According to the Brewer–Engle theory, the above results and discussion suggest that the hydrogen-evolving activity of Ni–Mo deposits should depend on these variables [5, 12, 13]. However, under the present electroplating conditions, the bath temperature and deposition current density possess no statistically significant effect on the hydrogen evolving activity of the Ni–Mo deposits. This is in contrast to the proposal that a higher plating temperature results in relatively poor quality deposits and that a higher current density should increase local pH in the cathodic diffusion layer, probably changing the Mo content in the deposits [14]. Since the composition of Ni–Mo deposits has been found to strongly depend on the applied current density and the bath temperature [23], the above results imply that the hydrogen-evolving activity of Ni–Mo deposits may not only depend on the Mo content but also on other textural properties (e.g., roughness, crystalline alloy, electronic characteristics etc.). Anyway, the bath temperature and the deposition current density were not considered in the steepest ascent study because these two variables do not exhibit significant effects on the activity for hydrogen evolution.

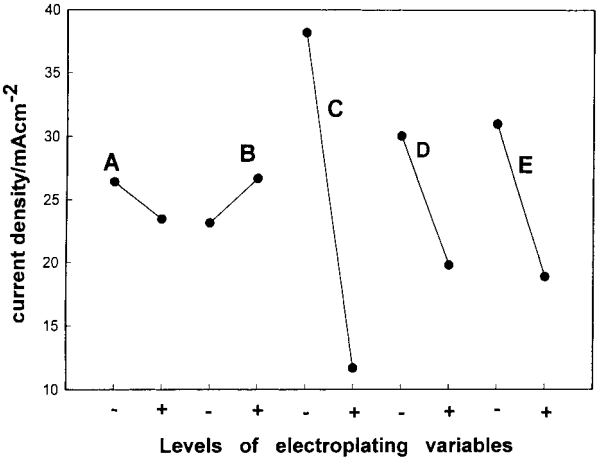

Fig. 1. Main effects of electroplating temperature (A), electroplating current density (B), pH (C), Ni/Mo ratio (D) and sodium citrate concentration (E) of the plating baths on the hydrogen-evolving activity of Ni–Mo deposits. (+) and (−) indicate the high and low levels of the these factors, respectively.

3.2. *Path of steepest ascent*

From the analysis of variance (ANOVA) and regression analysis of the results shown in Table 2, a fitted polynomial model can be generated. This model, quantitatively elucidating the effects of plating variables with statistical significance, is:

$$i = 24.95 - 13.25x_C - 5.13x_D - 6.05x_E + 5.31x_Cx_E + 3.56x_Ax_E - 3.55x_Bx_D \quad (1)$$

where x_i are the coded variables for factors A, B, C, D and E. The coded variables, x_i, are defined in standardized form as following [21]:

$$x_{i,\mathrm{HIGH}} = (X_{i,\mathrm{HIGH}} - X_{i,\mathrm{MEAN}})/S_i \ (= +1) \quad (2)$$

$$x_{i,\mathrm{LOW}} = (X_{i,\mathrm{LOW}} - X_{i,\mathrm{MEAN}})/S_i \ (= -1) \quad (3)$$

$$X_{i,\mathrm{MEAN}} = (X_{i,\mathrm{LOW}} + X_{i,\mathrm{HIGH}})/2 \quad (4)$$

$$S_i = (X_{i,\mathrm{HIGH}} - X_{i,\mathrm{LOW}})/2 \quad (5)$$

where $X_{i,\mathrm{HIGH}}$ and $X_{i,\mathrm{LOW}}$ are the high and low levels of the factor i, respectively. Note that in Table 3, the test

Table 3. Analysis of variance for the hydrogen evolving activity from 2^{5-1} fractional factorial design

Source	d.f.	SS	MS	F_0
C	1	2804.76	2804.76	55.55
D	1	420.25	420.25	8.32
E	1	585.64	585.64	11.60
AE	1	202.78	202.78	4.02*
BD	1	201.64	201.64	3.99*
CE	1	451.14	451.14	8.94
Error	9	454.44	50.49	
Total	15	5120.65		

$R^2 = 0.9112$
* Marginal significance

statistics, F, defined as MSF/MSE (MSF: mean squares of factors, MSE: mean squares of errors), are employed to test the statistical significance of each factor and the two-factor interactions. If the calculated value of F is greater than that in the F table at a specified probability level, a statistically significant factor or interaction is obtained. After the test, factors C, D and E, interactions CE, AE and BD exhibit statistically significant effects on the hydrogen-evolving activity of Ni–Mo deposits. However, the calculated F values of the AE and BD interactions are very close to the value on the F table at a specified probability level, indicated by asterisks. These two interactions should be located in the regions of marginal significance (i.e., their effects are not as important as the other four effects). Therefore, AE and BD interactions are also not considered in the steepest ascent study. The multiple correlation coefficient squared, $R^2 = 1 - (\mathrm{SSE}/\mathrm{SST})$, is the proportion of SST (sum of squares of total variances) explained by the fitted equation. A R^2 value close to 1 means a good fit to the experimental data ($R^2 = 0.9112$ in this model).

On the basis of Equation 1 and the above results, factors C (pH), D (Ni/(Ni + Mo) ratio), E (citrate concentration) and the CE interaction were the key electroplating variables affecting the activity of Ni–Mo deposits for hydrogen evolution. Thus, they are employed in the steepest ascent study. Note that the sign of coefficients for factors C and E are negative while that of their interaction is positive. Accordingly, the simultaneous movement in the negative direction for both factors C and E will have a synergistic effect on the hydrogen-evolving activity of Ni–Mo deposits.

On the basis of the steepest ascent methodology [21], the direction of the steepest ascent path is to simultaneously move $-13.25\ S_C$ and $-5.13\ S_D$ in the x_C and x_D directions, respectively for every $-6.05\ S_E$ in the x_E direction. Typical points on the steepest ascent path were studied in this work and are shown in Table 4, which suggest that the maximum of apparent current density for hydrogen evolution is located around the experimental settings of run 3. In Table 4 the apparent current density for hydrogen evolution rises sharply and decays from runs 2–4, indicating that the hydrogen evolving activity of Ni–Mo deposits should be a stiff function of one or more of the factors C, D and E. Since the pH of the plating solution was found to be the most significant factor in the FFD study, this factor is thus examined and confirmed to be the unusual variable influencing the hydrogen-evolving activity. It is worthy noting that in employing response surface methodology, the response variable (e.g., the apparent current density of hydrogen evolution in this work) is assumed to be a smooth function of the independent variables [20–22]. Accordingly, the pH of the plating bath has to be kept constant (pH 8) in the central composite design (CCD) because the apparent current density of hydrogen evolution is a stiff function of pH.

Table 4. Points on the path of steepest ascent

Run	Factor			i/mA cm^{-2}
	C	D	E/g l^{-1}	
1	11	5.55	103.67	7.17
2	9.5	4.42	90	18.79
3	8	3.29	76.33	97.29
4	6.5	2.16	62.66	6.21

3.3. *Central composite design*

Since the maximum of apparent current density of hydrogen evolution occurs around the experimental settings of run 3, the original (central) point of the CCD is set at run 3. The design factors and levels in the CCD study are shown in Table 5; meanwhile the design matrix with the corresponding results are listed in Table 6. Experiments on the original (central) point are repeated three times in order to evaluate the pure error between each experiment. In addition, data for exchange current density (i_0) and specific activity (i/q^*) of hydrogen evolution, and Mo/(Ni + Mo) ratio of the deposits are also presented in this Table, since the relationship between the Mo content and the specific (electrocatalytic) activity of Ni–Mo deposits were also examined in this work. The activity of runs 5–7 in Table 6 differs considerably from that of run 3 in Table 4. This significant difference is probably due to the presence of additives (saccharin ($C_7H_5NO_3S$), 0.2 g l^{-1} and *tetra*butyl-ammonium bromide, 0.1 g l^{-1}) in the plating baths of the CCD study, which smooth and reduce the active surface area of the Ni–Mo deposits.

Table 5. Factors and levels for the central composite design

Level	Factor	
	D	E/g l^{-1}
$-\sqrt{2}$	1.5	50
-1	2.03	57.61
0	3.3	76
$+1$	4.57	94.39
$+\sqrt{2}$	5.1	102

Table 6. Design matrix and experimental data of activity (i), exchange current density (i_0), specific activity (i/q^*) for hydrogen evolution, and Mo/(Ni + Mo) ratio of Ni–Mo deposits in the central composite design with a quadratic form fit

Run	Factor		i/mA cm^{-2}	i_0/μA cm^{-2}	(i/q^*)/A C^{-1}	Mo/(Ni + Mo)
	D	E				
1	−1	−1	95.50	16.60	4.207	0.28
2	−1	+1	56.80	5.64	16.608	0.39
3	+1	−1	96.61	13.04	8.863	0.26
4	+1	+1	61.24	8.27	14.546	0.30
5	0	0	87.47	14.16	9.159	0.29
6	0	0	88.92	13.42	9.651	0.30
7	0	0	88.13	12.70	9.792	0.28
8	0	$-\sqrt{2}$	116.36	18.67	4.155	0.26
9	0	$+\sqrt{2}$	47.64	3.79	16.149	0.34
10	$-\sqrt{2}$	0	58.61	4.38	11.864	0.41
11	$+\sqrt{2}$	0	79.07	11.76	7.907	0.34

For technological applications, apparent current density, predominantly governed by both the real surface area and the specific activity of electrocatalysts, is of practical importance. Yet, from a fundamental point of view, the investigation of electrocatalytic effects is also an important task, representing a guide to optimize the intrinsic activity of electrocatalysts. In order to identify the true catalytic effects of Ni–Mo deposits, comparisons must be carried out for unit real surface area. Since voltammetric charge, q^*, has been proposed to be proportional to electrochemically active surface area [8, 24], it is reasonable to believe that i/q^* represents normalized activity, taking into account variations in active surface area. Therefore, the voltammetric charge of $NiOOH/Ni(OH)_2$ transition is employed to represent the relative surface area in this work, and q^* is the total cathodic charge of the deposit on the negative sweep of a stabilized cyclic voltammogram measured in 1 M NaOH between 0 and 560 mV at 20 mV s^{-1}.

Data for apparent current density (i), exchange current density (i_0), and specific activity (i/q^*) of the HER, and Mo/(Ni + Mo) ratio of Ni–Mo deposits were subjected to regression analysis. From the analysis of variance for every regression coefficient, the term(s) without statistical significance was deleted from the full second-order model. The resultant second-order models corresponding to these four response variables were generated by the following:

$$i = 88.17 + 4.30\,x_D - 21.40\,x_E - 9.13\,x_D^2 \quad (6)$$

$$i_0 = 13.42 - 4.60\,x_E - 2.37\,x_D^2 \quad (7)$$

$$i/q^* = 9.50 + 0.45\,x_E + 4.38\,x_D^2 + 0.58\,x_E^2 - 1.68\,x_D x_E \quad (8)$$

$$\mathrm{Mo/(Ni + Mo)} = 0.292 - 0.026\,x_D + 0.033\,x_E + 0.035\,x_D^2 - 0.019\,x_D x_E \quad (9)$$

In fact, the magnitudes of coefficients on the same regression equation illustrate the relative effects of linear, quadratic, and interaction for the Ni/Mo ratio (x_D) and the sodium citrate concentration (x_E) in the plating solution. From a comparison of Equations 6, 7 and 9, on the one hand, there exists a negative correlation between the hydrogen evolving activity and the Mo/(Ni + Mo) ratio of deposits although there exist different terms on these three regression models. In other words, a Ni–Mo deposit with a higher Mo content, in general, has a lower apparent current density and exchange current density for hydrogen evolution within the investigation conditions. On the other hand, there is a positive relationship between the specific activity for hydrogen evolution and the Mo/(Ni + Mo) ratio since the sign of most coefficients in Equation 8 is consistent with that in Equation 9. Accordingly, the electrocatalytic activity of Ni–Mo deposits is qualitatively proportional to the Mo content, which is consistent with the prediction of the Engel–Brewer valence-bond theory [5, 12, 13], although the x_D and x_E^2 terms in Equation 9 are not found in Equation 8.

The analysis of variance (ANOVA) for apparent current density, exchange current density and specific activity for hydrogen evolution, and Mo/(Ni + Mo) ratio in the deposits have been carried out. All ANOVA data show that the regressed Equations 6–9 are 'statistically significant' since the calculated values of test statistics, F (29.52, 9.31, 15.45 and 13.13 for Equations 6–9, respectively), are much larger than that in the F table at a specified probability level. In addition, the R^2 values for Equations 6–9 are 0.9672, 0.9030, 0.9392 and 0.9292, respectively. The above results indicate that Equations 6–9 accurately represent the dependence of apparent current density, exchange current density and specific activity of hydrogen evolution, and Mo/(Ni + Mo) ratio of the deposits on factors D and E.

3.4. *Contour plots*

The contour plots of all response variables against Ni/Mo ratio (x_D) and sodium citrate concentration (x_E) in the plating bath were constructed using their corresponding regression models (i.e., Equations 6–9), which facilitate a straightforward examination of the dependence of these response variables on the plating vari-

ables. Typical contour diagrams for activity (i), exchange current density (i_0), and specific activity (i/q^*) of hydrogen evolution, and the Mo/(Ni + Mo) ratio of the deposits are shown in Figures 2–5, respectively.

In Figure 2 the apparent current density of hydrogen evolution, gradually increases with decreasing citrate concentration (i.e., x_E) in the bath. In addition, an extremal region with maximum i ($\sim$118 mA cm^{-2}) occurs at a citrate concentration of 50 g l^{-1} and a Ni/Mo ratio close to 3.3. The maximum activity is about three times the minimum activity (occurring, respectively, at a Ni/Mo ratio of 1.5 and a citrate concentration of 102 g l^{-1}), revealing the contribution of the plating variables under present investigation conditions. It is worth noting that from a comparison of Figures 2 and 3, the effects of Ni/Mo ratio and citrate concentration on the apparent current density and the exchange current density (i.e., activity at the equilibrium potential) of hydrogen evolution are approximately the same. This trend is attributable to the fact that the log i/E curves of all Ni–Mo deposits in the CCD study are in parallel (not shown here). This result implies the same mechanism and rate-determining step of the HER on these Ni–Mo deposits.

In Figure 4, the extremal region with minimum i/q^* ($\sim$10 A C^{-1}) occurs at a Ni/Mo ratio close to 3.3 and a citrate concentration between 57 and 94 g l^{-1}. This region is very close to the preparation conditions possessing the maximum hydrogen-evolving activity (i.e., a Ni/Mo ratio of 3.3 and a citrate concentration of 50 g l^{-1}, respectively). In addition, the extremal region with maximum i/q^* ($\sim$25 A C^{-1}) occurs at a Ni/Mo ratio of 1.5 and a sodium citrate concentration of 102 g l^{-1}, respectively, which is the same plating settings exhibiting the minimum hydrogen-evolving activity. From the above results, the maximum activity of Ni–Mo deposits for hydrogen evolution should be mainly caused by a relatively high surface area, which can be prepared at a citrate concentration of 50 g l^{-1} and a Ni/Mo ratio of 3.3, respectively.

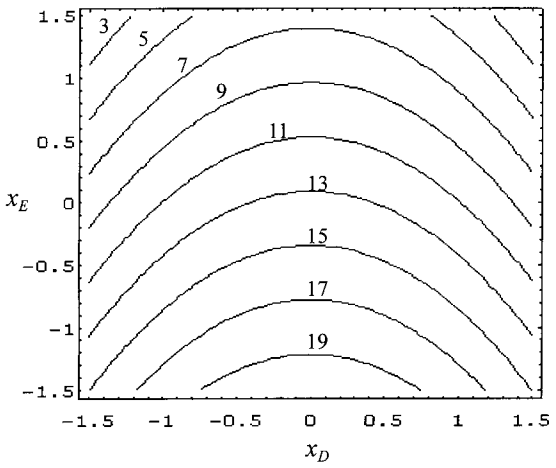

Fig. 3. Contour lines for constant exchange current density of hydrogen evolution on Ni–Mo deposits against the Ni/Mo ratio (x_D) and the sodium citrate concentration (x_E) in plating baths.

From an examination of Figure 5, the dependence of the Mo content within Ni–Mo deposits on both the citrate concentration and the Ni/Mo ratio is very complicated. In general, the Mo content increases with decreasing the Ni/Mo ratio in the plating baths. However, since citrate ion can form complexes with both MoO_4^{2-} and Ni^{2+} [14, 16], it is reasonable to propose the existence of interactive effects between the Ni/Mo ratio and the citrate concentration on the Mo content during the Ni–Mo induced codeposition. An extremal region with minimum Mo/(Ni + Mo) ratio ($\sim$0.25) occurs at the same experimental settings corresponding to the maximum hydrogen-evolving activity (i.e., a citrate concentration of 50 g l^{-1} and a Ni/Mo ratio of 3.3, respectively). In addition, the extremal region with maximum Mo/(Ni + Mo) ratio is located in the same experimental settings corresponding to the minimum apparent current density of hydrogen evolution. Therefore, a Ni–Mo deposit with a higher Mo content, in general, has a lower activity and exchange

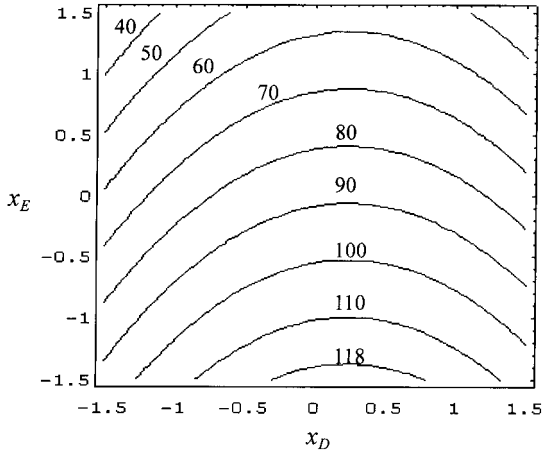

Fig. 2. Contour lines for constant activity of Ni–Mo deposits for hydrogen evolution at $\eta \approx 230$ mV against the Ni/Mo ratio (x_D) and the sodium citrate concentration (x_E) in plating baths.

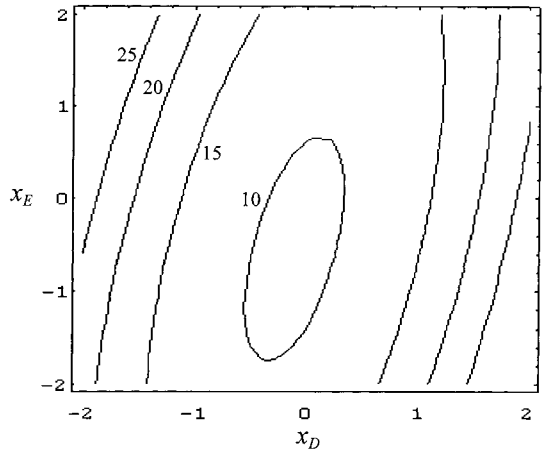

Fig. 4. Contour lines for specific activity (i/q^*) of Ni–Mo deposits for hydrogen evolution against the Ni/Mo ratio (x_D) and the sodium citrate concentration (x_E) in plating baths.

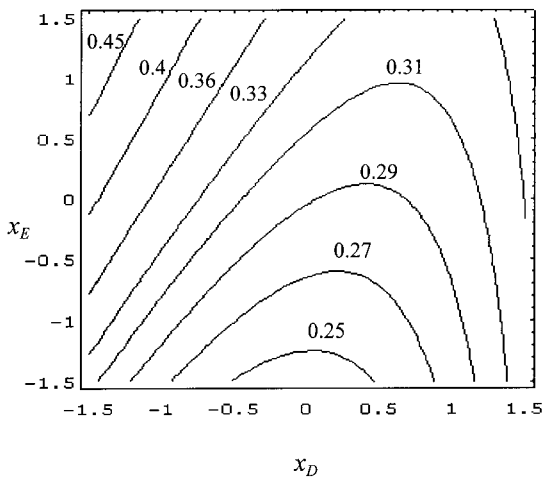

Fig. 5. Contour lines for constant Mo/(Ni + Mo) ratio within Ni–Mo deposits against the Ni/Mo ratio (x_D) and the sodium citrate concentration (x_E) in plating baths.

current density of hydrogen evolution, which is reasonably attributed to the surface area effect.

A comparison of Figures 4 and 5 reveals that the maximum specific activity of hydrogen evolution occurs at the same electroplating settings possessing the maximum Mo/(Ni + Mo) ratio, revealing the effect of composition on the intrinsic activity of Ni–Mo deposits for the HER. From all the above results, a combined effect of composition and real surface area of Ni–Mo deposits results in the optimum activity of the activated cathodes for hydrogen evolution.

From the results and discussion in Figure 2, the Ni–Mo deposits prepared from the plating baths with a Ni/Mo ratio of 3.3 and a sodium citrate concentration below 50 g l^{-1} are expected to possess a higher activity (>120 mA cm^{-2}) for the HER. This prediction was confirmed and the results are shown in Table 7. The hydrogen-evolving activity reached a maximum when the Ni–Mo deposit was electroplated from the bath with a Ni/Mo ratio of 3.3 and a sodium citrate concentration of 40 g l^{-1}, respectively. Accordingly, the regression models proposed in this work are acceptable. A green and gel-like precipitate of nickel hydroxide was found when the concentration of sodium citrate in the plating bath was ≤30 g l^{-1}. The above result indicates the disappearance of a stable complex bath when the concentration of sodium citrate was below 30 g l^{-1}. This causes precipitation of free Ni ions and results in a change in the effective concentration of Ni-citrate complex species in the plating baths, likely causing changes in textural properties and hydrogen evolving activity of Ni–Mo deposits.

Table 7. Points of confirmation for Ni–Mo deposits possessing the maximum activity for hydrogen evolution

Run	Ni/Mo ratio	Sodium citrate/g l^{-1}	i/mA cm^{-2}
1	3.3	50	119.37
2	3.3	45	127.89
3	3.3	40	141.53
4	3.3	35	126.41
5	3.3	30	119.89

4. Conclusions

Using the sequential experiment strategies (i.e., fractional factorial design, path of steepest ascent, and response surface methodology coupled with central composite design), the key factors in the Ni–Mo induced deposition affecting the hydrogen-evolving activity of Ni–Mo deposits are pH, Ni/Mo ratio, and citrate concentration in the plating baths. The activity of Ni–Mo deposits for hydrogen evolution was found to be a stiff function of pH of the plating bath. Nickel-molybdenum deposits with the highest apparent current density of hydrogen evolution were electroplated from a bath with a pH of 8, a Ni/Mo ratio of 3.3, and a sodium citrate concentration of 40 g l^{-1}, respectively. Nickel–molybdenum deposits with the maximum Mo/(Ni + Mo) ratio possessed the maximum specific activity for the hydrogen evolution reaction while the predominant effect determining the activity of Ni–Mo deposits for hydrogen evolution is real surface areas of the deposits.

Acknowledgements

The financial support of this work, by the National Science Council of the Republic of China under contract NSC 88-2214-E-194-007, is gratefully acknowledged.

References

1. K.E. Cox and K.D. Williamson, Jr. (Eds), 'Hydrogen: Its Technology and Implications', (CRC Press, 1979).
2. D.E. Brown, M.N. Mahmood, A.K. Turner, S.M. Hall and P.O. Fogarty, *Int. J. Hydrogen Energy* **7** (1982) 405 and references cited therein.
3. R. Kötz and S. Stucki, *J. Appl. Electrochem.* **17** (1987) 1190.
4. T. Takahashi, *in* T. Ohta (Ed.), 'Solar Hydrogen Energy Systems' (Pergamon Press, New York, 1979), p. 35.
5. C. Fan, D.L. Piron, A. Sleb and P. Paradis, *J. Electrochem. Soc.* **141** (1994) 382.
6. J. Stevanovic, S. Gojkovic, A. Despic, M. Obradovic and V. Nakic, *Electrochim. Acta* **43** (1998) 705.
7. H. Yamashita, T. Yamamura and K. Yoshimoto, *J. Electrochem. Soc.* **140** (1993) 2238.
8. C.-C. Hu, C.-Y. Lin and T.-C. Wen, *Mat. Chem. Phys.* **44** (1996) 233.
9. S.A.S. Machado and L.A. Avaca, *Electrochim. Acta* **39** (1994) 1385 and references cited therein.
10. I. Paseka, *Electrochim. Acta* **38** (1993) 2449.
11. I. Arul Raj and K.I. Vasu, *J. Appl. Electrochem.* **20** (1990) 32.
12. H. Ezaki, M. Morinaga and S. Watanabe, *Electrochim. Acta* **38** (1993) 557.
13. M.M. Jaksic, *Electrochim. Acta* **29** (1984) 1539.
14. A. Brenner, 'Electrodeposition of Alloys', Vols 1–2 (Academic Press, New York, 1963).

15. E.J. Podlaha and D. Landolt, *J. Electrochem. Soc.* **143** (1996) 885 and 893.
16. E. Uekawa, K. Murase, E. Matsubara, T. Hirato and Y. Awakura, *J. Electrochem. Soc.* **145** (1998) 523.
17. E.J. Podlaha and D. Landolt, *J. Electrochem. Soc.* **144** (1997) 1672.
18. D.W. Ernst and M.L. Holt, *J. Electrochem. Soc.* **105** (1958) 686.
19. E. Chassaing, K. Vu Quang and R. Wiart, *J. Appl. Electrochem.* **19** (1989) 839.
20. G.E.P. Box, W.G. Hunter and J.S. Hunter, 'Statistics for Experiments' (J. Wiley & Sons, New York, 1978), p. 374.
21. J.A. Cornell, 'How to Apply Response Surface Methodology', Vol. 8 (ASQC, Wisconsin, 1990).
22. D.C. Montgomery, 'Design and Analysis of Experiments', 4th edn (J. Wiley & Sons, Singapore, 1997).
23. D.W. Ernst, R.F. Amlie and M.L. Holt, *J. Electrochem. Soc.* **102** (1955) 463.
24. T.-C. Wen, C.-C. Hu and Y.-J. Li, *J. Electrochem. Soc.* **140** (1993) 2554.